Letter

Dynamical beats of short pulses in waveguide QED

Dianqiang Su,[1,2] Yuan Jiang,[1,2] Silvia Cardenas-Lopez,[3] Ana Asenjo-Garcia,[3] Pablo Solano,[4,5] Luis A. Orozco,[6] and Yanting Zhao[1,2]

[1]*State Key Laboratory of Quantum Optics and Quantum Optics Devices, Institute of Laser Spectroscopy, Shanxi University, Taiyuan 030006, People's Republic of China*

[2]*Collaborative Innovation Center of Extreme Optics, Shanxi University, Taiyuan 030006, People's Republic of China*

[3]*Department of Physics, Columbia University, New York, New York 10027, USA*

[4]*Departamento de Física, Facultad de Ciencias Físicas y Matemáticas, Universidad de Concepción, Concepción, Chile*

[5]*Departamento de Física, Azrieli Global Scholars Program, CIFAR, Toronto, Canada*

[6]*Joint Quantum Institute, Department of Physics and NIST, University of Maryland, College Park, Maryland 20742, USA*

(Received 21 April 2023; accepted 29 September 2023; published 18 December 2023)

We study weak pulse propagation through near-resonant collective media. The timescales of the pulse and the lifetime of the media are comparable. The transmitted pulse develops temporal oscillations, known as dynamical beats. We use a collection of ^{133}Cs atoms randomly captured by a nanofiber-based optical lattice. An effective macroscopic model derived from a microscopic many-atom input-output theory reproduces the observations. The results deepen our understanding of single-photon pulse propagation, crucial for many waveguide QED-based quantum information protocols.

DOI: 10.1103/PhysRevResearch.5.L042041

I. INTRODUCTION

Light pulses traveling through waveguides make high-speed communication possible and present us with potential routes for processing quantum information. Understanding the effects of light pulses propagating through ensembles of resonant emitters in a one-dimensional waveguide becomes crucial for many quantum information applications [1–4], especially for light pulses whose time duration is comparable to the lifetime of the atomic qubits. Such study has a long history in physics and engineering. Early work by Sommerfeld [5] and Brillouin [6,7] showed the existence of what is now known as precursors [8–11], observed when the rise time of a pulse is shorter than the lifetime of the excited state of the resonant media [12–15], whose quantum properties have been recently studied with Rydberg atoms [16,17]. Pulses propagating through a resonant media also show amplitude oscillations, as observed by Lynch *et al.* on Mössbauer spectroscopy [18] and explained with a quantum theory by Harris [19]. These oscillations are called dynamical beats (DBs) [20], most noticeably appearing in Mössbauer experiments [21] but also present in the optical regime [22–24]. DBs are affected by the collective atomic response of the media, superradiantly speeding up the initial decay [25–28] and subradiantly slowing down the long-time behavior. Novel quantum information protocols in the context of waveguide quantum electrodynamics (QED) [29] are based on pulse propagation [1–4], bringing a renewed interest in these phenomena [30].

Here, we experimentally and theoretically study the evolution of a weak light pulse confined in a waveguide crossing an ordered array of atoms, as depicted by Fig. 1(a). In particular, we focus on the limit of single-photon resonant pulses with a temporal width shorter than the atomic lifetime, a relevant regime for quantum information protocols in waveguide QED. We observe a sharp division in the resulting temporal behavior: at short times, while the pulse is still in the medium, there is a buildup of a macroscopic polarization (exciting atoms into a superposition). After that, the transmitted pulse is determined by the radiative decay of the macroscopic polarization (or collective atomic radiation) [30–33]. A transmission dip, or zero, distinctively separates both regimes, denoting the moment when the induced polarization amplitude matches the electric field amplitude of the input pulse but with the opposite phase.

In the single-photon regime, the dynamics of the pulse is accurately described by means of a single parameter (the optical depth), greatly simplifying the theoretical description of the problem. While the severe pulse modification challenges practical implementations of quantum information protocols, it also presents an opportunity for shaping the amplitude and phase of propagating pulses in waveguide QED platforms.

II. EXPERIMENTAL SETUP

Hundreds of cesium (Cs) atoms are optically confined around the surface of an optical nanofiber [34]. The nanofiber is 500 nm in diameter over a length of 5 mm fabricated from a standard optical fiber by the flame brushing technique [35] [see Figs. 1(a) and 1(b)]. The fiber sustains a single spatial

Published by the American Physical Society under the terms of the Creative Commons Attribution 4.0 International license. Further distribution of this work must maintain attribution to the author(s) and the published article's title, journal citation, and DOI.

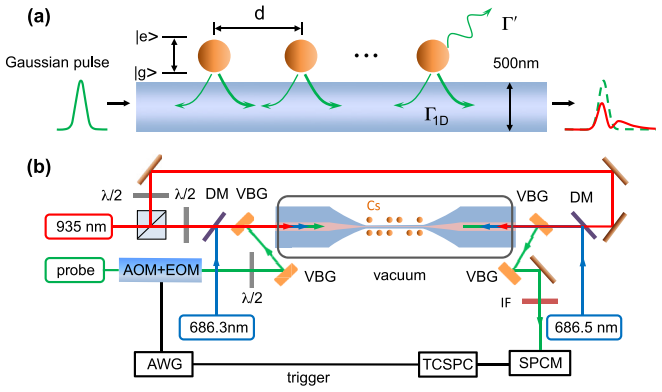

FIG. 1. (a) The atomic array is trapped in the evanescent field of an optical lattice near the nanofiber surface. The lattice constant d is half the wavelength of the trapping light. The temporal shape of a Gaussian input pulse (green) gets modified after propagating through an array of trapped atoms (red). (b) Schematic of the apparatus includes dichroic mirrors (DMs), volume Bragg gratings (VBGs), and half wave plates ($\lambda/2$) with the pulses coming from the left detecting them with a single-photon counter module (SPCM) on the right. The pulses are produced by acousto- and electro-optical modulators (AOM, EOM) controlled by an electronic pulse from an arbitrary wave generator (AWG) that triggers the time correlator for single-photon counters (TCSPCs) for further data processing.

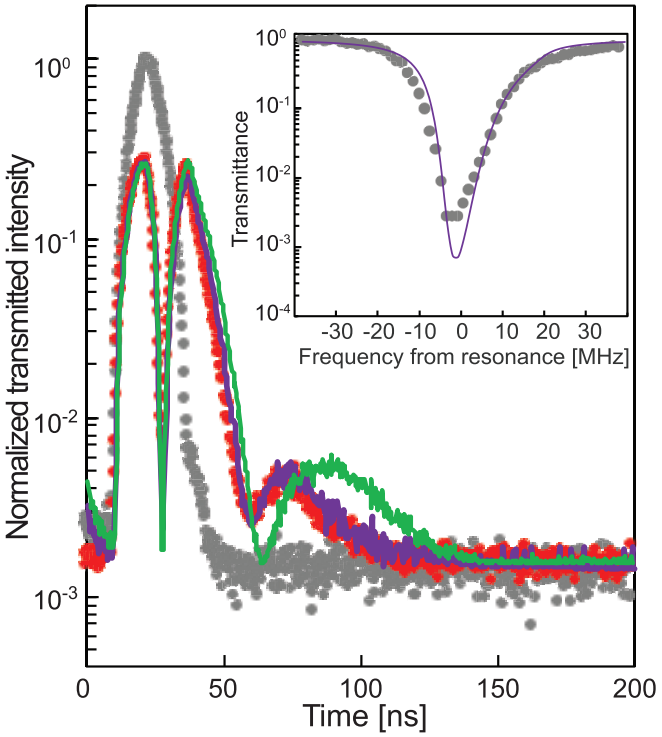

FIG. 2. Time dependence of the transmitted intensity (red) for a 10 ns FWHM pulse propagating in a medium of OD = 11.6, normalized by the peak intensity of the pulse without atoms (gray), in logarithmic scale. The solid green line shows the results for the multimode model with an ideal single Lorenzian absorption as input. The solid purple line shows the results of the model using a broadened absorption modeled by a sum of Lorentzians. The inset shows the measured absorption (gray dots) and the result of the sum of Lorenzians (solid gray line). Note the logarithmic vertical scale. In all plots, $\Gamma'/2\pi = 5.2$ MHz.

electromagnetic mode. We use a two-color optical dipole trap [36], operating at (red) 935 nm and (blue) 686.3 and 686.5 nm, to reduce the Stark shift and longitudinal circular polarization on the trapped atoms [37,38], close to the magic wavelengths [39]. The calculated coupling of a trapped atom into the waveguide mode is $\Gamma_{1D} \approx 0.03\Gamma'$, with Γ' the emission rate into free space, for the operating transition $6S_{1/2}, F = 4 \rightarrow 6P_{3/2}, F = 5$. A magneto-optical trap captures Cs atoms from the residual gas in the vacuum chamber, which then fall into the dipole traps around the nanofiber. The lifetime of trapped atoms in the nanofiber optical lattice is about 8 ms, which is used to extract the value of the optical depth (OD), by different delay times, after loading into the nanofiber dipole trap. Although the OD (measured by absorption spectroscopy) is reproducible, the exact location of the atoms within the periodic lattice is not. The influence of this disorder has been thoroughly studied in Ref. [30] and it is not an issue in the present work.

A combination of a fiber EOM (Ixblue, NIR-MX800-LN-10-00-P-P-FA-FA) and AOM (AA Opto Electronic MT110-B50A1-IR) allows for shaping the pulses, changing their characteristic rise and fall times. We limit the length of the pulses to less than $1/\Gamma'$, the natural atomic lifetime. An electronic reference triggers the optical pulse and sets the zero time. A data acquisition card (Siminics FT1040) time stamps the electronic pulses from the detectors (Excelitas SPCM-AQRH-14-F) for further data processing. The power of the excitation, which is small compared to the saturation intensity, corresponds to an average of ≈0.4 photons per pulse, guaranteeing less than two photons 94% of the time. For a given OD, we repeat the process of preparation, excitation, and measurement 5000 times to obtain good statistics. The corresponding input and transmitted pulses are shown in Fig. 2.

III. THEORETICAL MODEL

Generically, the transmitted field reads

$$E(t) = \frac{1}{2\pi}\int_{-\infty}^{\infty} \mathcal{T}(\omega)E_0(\omega)e^{-i\omega t}d\omega, \tag{1}$$

where $E_0(\omega)$ is the Fourier transform of the input pulse, and $\mathcal{T}(\omega)$ is the transmission coefficient of the waveguide in the presence of atoms.

We obtain the transmission coefficient via an input-output theory that enables us to write the (linear) response of the system in terms of N collective atomic modes, where N is the atom number [40,41]. These modes, which can be either super- or subradiant, emerge from the atom-atom interactions mediated by the waveguide. They are found by diagonalizing the single-excitation sector of the non-Hermitian Hamiltonian,

$$\mathcal{H}_{1D} = -i\frac{\hbar\Gamma_{1D}}{2}\sum_{i,j=1}^{N} e^{ikd|i-j|}\hat{\sigma}_{eg}^{i}\hat{\sigma}_{ge}^{j}. \tag{2}$$

Here, k is the guided-mode wave vector, d is the interatomic separation, and $\hat{\sigma}_{ge}^{j} = |g_j\rangle\langle e_j|$ is the coherence operator for atom j.

Plugging the steady-state solution of the Heisenberg-Langevin equations for the atomic coherences into an input-output equation for a monochromatic electromagnetic field, the transmission coefficient is found to be [40]

$$\mathcal{T}(\omega) = 1 - \frac{i\Gamma_{1D}}{2}\sum_{\xi=1}^{N}\frac{\eta_\xi}{\omega-\omega_0+i\Gamma'/2-\lambda_\xi}. \tag{3}$$

Here, ω_0 is the atomic resonance frequency and $\{\lambda_\xi\}$ are the (single-excitation) eigenvalues of $\mathcal{H}_{1D}$, which encode the frequency shifts and decay rates of the collective modes. The parameter $\eta_\xi = \sum_{n,m=1}^{N} v_{\xi,n}v_{\xi,m}e^{-ikd(n-m)}$ denotes the spatial overlap of the external field with the eigenvector $\mathbf{v}_\xi$. The expression for the transmission coefficient arising when atoms are in the "mirror configuration" (for which kd is an integer multiple of π) is quite simple. In this configuration, there is only a single superradiant mode and the Heisenberg-Langevin equations are identical to those of a collection of atoms interacting with a single-cavity mode in the low-intensity and bad-cavity limits of the cavity QED work of Carmichael *et al.* [42] (see Appendix A).

The output field is the sum of the input field, $E_0(t)$, and the scattered field by the different collective modes. For an input pulse with peak intensity I_0 and a Gaussian temporal envelope of variance σ^2, i.e., $f(t) = e^{-t^2/\sigma^2}/\sqrt{2\pi\sigma^2}$, the transmitted intensity reads (see Appendix A)

$$\frac{I_d(t)}{I_0} = \left| f(t)e^{-i\Delta t} - \frac{\Gamma_{1D}}{4}\sum_{\xi=1}^{N} a_\xi e^{-(i\lambda_\xi+\Gamma'/2)t}\,\mathrm{erfc}\left(\frac{b_\xi - t}{\sqrt{2}\sigma}\right)\right|^2, \tag{4}$$

where $\Delta = \omega_p - \omega_0$ is the detuning between the central frequency of the pulse and the atomic resonance frequency, $\mathrm{erfc}(\cdot)$ is the complementary error function, and a_ξ and b_ξ are expressions given in Appendix A.

The first zero in Fig. 2 appears when the two terms in Eq. (4) cancel each other. In the limit of large optical depth (i.e., for $\mathrm{OD} \equiv 2N\Gamma_{1D}/\Gamma' \gg 1$), the first zero appears at short times compared to the natural lifetime $1/\Gamma'$. In the crude limit of considering only the most superradiant mode (with decay rate $\sim N\Gamma_{1D}$), a Taylor expansion of the above expression allows us to find the time for the first zero as $\Gamma'\tau_{\mathrm{zero}} \simeq 4/\mathrm{OD}$. The subsequent zeros, i.e., the dynamical beats, arise from interference between different collective atomic modes. However, the phenomenology cannot be simply attributed to a few dominant modes; it is truly a multimode feature.

In the large-atom limit, the transmission coefficient in Eq. (3) converges to that of a continuous medium [30], i.e.,

$$\mathcal{T}(\omega) = \exp\left(-\frac{iN\Gamma_{1D}}{2}\frac{1}{\omega-\omega_0+i\Gamma'/2}\right). \tag{5}$$

The above transmission coefficient allows for a semianalytical expression of the transmitted pulse intensity. The details are fully developed in Ref. [30], where we investigate the transport of broadband square photon pulses in waveguide QED, and the calculation is inspired by Ref. [19]. Here we adapt these results to Gaussian input pulses. After performing the integral in frequency, the output intensity can be written as series of Bessel functions, i.e.,

$$\frac{I_d(t)}{I_0} = e^{-\Gamma' t}\left|\sum_{m=-\infty}^{\infty} A_m\left(\sqrt{\frac{t}{\mathrm{OD}\Gamma'}}\right)^m J_m(\sqrt{\mathrm{OD}\Gamma' t})\right|^2, \tag{6}$$

where the expressions for the coefficients A_m—which depend on the pulse parameters—are given in Appendix A.

As can be seen from this expression, the optical depth determines the timescale of the dynamics. Moreover, while our Eq. (2) refers to an ordered array, the convergence of the transmission coefficient to that of a continuous medium for large-atom number indicates that position disorder is irrelevant for our results. This last point is in contrast with what occurs for reflection, which is only observable in periodic arrays [43–45].

IV. EXPERIMENTAL ANALYSIS

We excite the array of atoms with a Gaussian pulse, depicted in gray in Fig. 2. The number of incident photons per pulse is kept around 0.4. The transmitted pulse, shown in Fig. 2, has three peaks and two valleys, from DBs. The first valley is reproduced by the model even in the limit of a single electromagnetic mode coupled to a single collective atomic mode, which is equivalent to only considering the nanofiber electromagnetic mode and a single atom. It shows the interference between the two with a significant decrease in the transmission.

The second valley requires the many-atom theory (green line) with its many modes. This theory also captures the relatively fast decay on the way to the second valley. To produce the theory curve, we solve the Heisenberg-Langevin equations for the atomic coherences for the input drive (which we extract from the experiment). We then compute the transmitted field via input-output equations.

The amplitude of the third peak is correctly predicted by the many-atom theory, but it emerges later in the calculation than in the measurement. An exploration of the numerical simulations shows that this discrepancy is due to line broadening. To account for this disparity, we model the complex transmission coefficient of the asymmetrically and inhomogeneously broadened atomic medium as the product of frequency-displaced transmission coefficients of the form of Eq. (5), each with a different number of atoms (see Appendix B for details). The number of atoms corresponding to each shifted transmission is sampled from a log-normal distribution [46], characteristic of random processes bounded on one side, such as position-dependent, positive-only light shifts. The model reproduces to a good approximation the measured transmission spectrum shown in the inset of Fig. 2. Considering the modeled transmission coefficient, we produce the purple line from the square of Eq. (1), in excellent agreement with the pulse measurements.

Figure 3 shows the location of the first zero from the turn-on of the excitation pulse and the slope of the second fall from a series of pulse transmission measurements, as a function of the optical depth. Two sets of data, corresponding to pulses of 10 ns (blue circle) and 13 ns FWHM (red square), show the delay of the first zero as a function of OD. The theory curves (red, blue), as obtained from the many-atom theory,

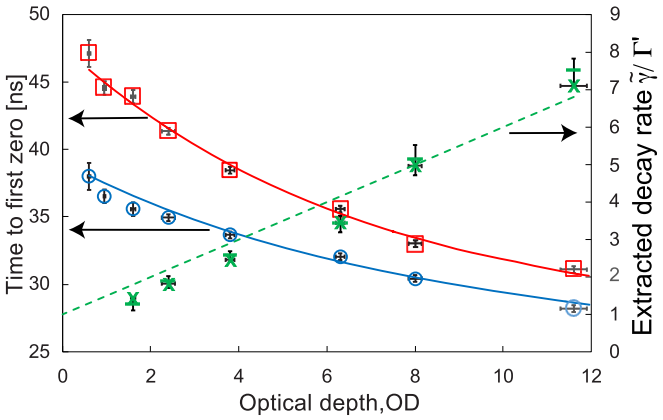

FIG. 3. Left: Evolution of the first zero with on-resonance excitation (valley) of the transmission as a function of the OD for two different pulse widths. Blue circles correspond to a FWHM of 10 ns and the red squares for a FWHM of 13 ns. The corresponding blue and red continuous lines indicate the prediction of the full theory. Right: Extracted decay rate (green) from the fall of the second peak when the input is a 10 ns pulse (bars), 13 ns (x's). The dashed green line is 1+OD/2, the expected value from the theory. The error bars are the same for the two sets of data, but only the horizontal or the vertical are plotted for clarity.

agree with the experimental data. The curves are produced with a single adjustable parameter, i.e., the offset from the peak of the input pulse (1.1 ns optimizes the fit). As expected, the time of the first zero decreases with increasing optical depth. The dependence on the pulse width becomes less relevant as the optical depth increases, in agreement with our theoretical model (which predicts that the first zero occurs at a time $\Gamma'\tau_{\rm zero} \simeq 4/\mathrm{OD}$ after the input pulse center in the large OD limit). However, while the theory captures well the scaling with the optical depth, the approximation that yields a simple expression is only in qualitative (but not quantitative) agreement, as the OD in the experiment is not large enough.

The right axis of Fig. 3 shows an effective decay rate obtained from a fit of the second fall on the transmitted pulses of 10 ns (bars) and 13 ns (x's). Both data sets have statistical error bars and only one of them is plotted for clarity. The extracted numbers fall in the same range. The rate value seems to only be dependent on the OD. Once the absorption is large enough, the decay rate grows almost linearly with the increased OD. An enhanced decay rate arises because the superradiant modes in Eq. (4) dominate the signal at early times. By assuming that the decay rate is determined by these modes, we obtain $\tilde{\gamma} \sim \Gamma'(1 + \mathrm{OD}/2)$, which is consistent with the experimental results. The decay rate changes at later times, but experimental noise prevents us from accessing this regime.

V. DISCUSSION

We measured the emergence of oscillations in the temporal behavior of a pulse in the single-photon limit as it propagates in a waveguide through a resonant atomic medium. We find that the position of the first valley and the first two peaks is quite insensitive to the absorption details near resonance. This is because the transmittance is practically zero near resonance. On the other hand, the tails of the spectral distribution contribute much more to the second valley and third peak. Although good from a statistical point of view, the fits to the measured absorption spectrum present deviations in the tails. Combinations of the many magnetic sublevels, the position-dependent light shifts induced by the trap, the remaining heating of the trapped atoms, and the nanofiber torsional modes [47] can contribute to this issue.

In the waveguide QED regime amenable to nanofiber experiments, a quantum description for the atomic response is not needed to quantitatively understand DBs. Although our approach comes from a microscopic description [30], in the many-atom limit, the results agree perfectly with those predicted for a continuous medium. This result shows that a classical description based on the linear transmission coefficient (for a continuous medium) and input electric field is sufficient in many waveguide QED transmittance measurements [31–33], in particular when both the saturation and the ratio Γ_{1D}/Γ' are low.

Single photons interacting with quantum emitters are the basis of several quantum information processing protocols [1–4]. Realistic implementations of such protocols can suffer from misshaping of the photon pulse shape, an unintended result of the photon-emitter interaction. Our results present tools to identify and address this platform-dependent potential source of error. Furthermore, some applications can benefit from amplitude and phase modulation of the pulse. These modulations can be achieved by controlling the spectral properties of the near-resonant media, as the presented theory and experiments show.

VI. CONCLUSION

We experimentally and theoretically study the problem of pulse propagation through a resonant media, showing the emergence of dynamical beats in waveguide QED. We focus on the limit of pulses with temporal widths below the atomic lifetime $1/\Gamma'$ and below the atomic saturation intensity. In order to understand the most relevant features in the emergence of dynamical beats, we propose a theoretical effective model based on macroscopic electrodynamics, which can be microscopically derived from a multiple-scattering input-output theory. Our results provide insights into the key factors determining the emergence of dynamical beats, a relevant effect for light-based communication and information processing protocols that relies on sending pulses to interconnect resonant samples or quantum emitters.

ACKNOWLEDGMENTS

P.S. is a CIFAR Azrieli Global Scholar in the Quantum Information Science Program. This work was supported by the National Key Research and Development Program of China (Grant No. 2022YFA1404201), National Natural Science Foundation of China (Grants No. 12034012, No. 12274272, No. 61827824, No. 62105191, No. 12074231), Fundamental Research Program of Shanxi Province (Grant No. 20210302124537), "1331 KSC", PCSIRT (Grant No. IRT_17R70), 111 Project (Grant No. D18001), CONICYT-PAI Grant No. 77190033, and FONDECYT Grant No.

11200192 from Chile. We also gratefully acknowledge support from the Air Force Office of Scientific Research through their Young Investigator Prize (Grant No. 21RT0751), the National Science Foundation through their CAREER Award (Grant No. 2047380), the A. P. Sloan Foundation, and the David and Lucile Packard Foundation. S.C.-L. acknowledges additional support from the Chien-Shiung Wu Family Foundation.

APPENDIX A: THEORY

1. Many-atom theory

An ensemble of N two-level atoms coupled to a waveguide and driven by a weak pulse with an arbitrary temporal shape $\Omega(t)$ is described by the effective Hamiltonian $\mathcal{H} = \mathcal{H}_{1D} + \mathcal{H}' + \mathcal{H}_{\text{drive}}$, where

$$\mathcal{H}_{1D} = -i\frac{\hbar\Gamma_{1D}}{2}\sum_{i,j=1}^{N} e^{ikd|i-j|}\hat{\sigma}_{eg}^{i}\hat{\sigma}_{ge}^{j}, \tag{A1a}$$

$$\mathcal{H}' = -i\frac{\hbar\Gamma'}{2}\sum_{i=1}^{N}\hat{\sigma}_{ee}^{i}, \tag{A1b}$$

$$\mathcal{H}_{\text{drive}} = -\hbar\Delta\sum_{i=1}^{N}\hat{\sigma}_{ee}^{i} - \hbar\Omega(t)\sum_{i=1}^{N}\left(e^{ikz_i}\hat{\sigma}_{eg}^{i} + \text{H.c.}\right). \tag{A1c}$$

Here, k, Δ, and $\{z_i\}$ are, respectively, the light wave vector, the detuning between the central frequency of the drive and the atomic resonance, and the set of atomic positions along the waveguide. The expectation value of the atomic coherences, $\langle\hat{\sigma}_{ge}^{n}\rangle \equiv \sigma_{ge}^{n}$, evolves according to

$$\dot{\sigma}_{ge}^{n} = i\left(\Delta + i\frac{\Gamma'}{2}\right)\sigma_{ge}^{n} + i\Omega(t)e^{ikz_n} - \frac{\Gamma_{1D}}{2}\sum_{m=1}^{N} e^{ik|z_n - z_m|}\sigma_{ge}^{m}. \tag{A2}$$

The expectation value for (the positive-frequency component of) the electric field at a point to the left of the ensemble is a sum of the input field and the field generated by the atoms,

$$E^{+}(z,t) = \Omega(t)e^{ikz} + i\frac{\Gamma_{1D}}{2}\sum_{i=1}^{N} e^{ik|z-z_i|}\sigma_{ge}^{i}(t). \tag{A3}$$

The results presented in Fig. 2 are calculated by numerically solving Eq. (A2) using the amplitude of the experimental pulse as $\Omega(t)$, for 40 disordered atoms with OD = 11.6 and $\Gamma_{1D}/\Gamma' = \text{OD}/2N$. As discussed in the main text, the output field is determined solely by $N\Gamma_{1D}$ in the large-atom limit, so the specific number of atoms and its configuration are irrelevant as long as $N \gg 1$. Noise has been added to the final result (see Appendix C for details) to make the experimental signal and the simulation agree at long times (due to the logarithmic scale, this is a small correction at short times).

2. Transmitted intensity in terms of collective modes

The system of equations in Eq. (A2) is simpler if we transform to the basis that diagonalizes the atom-atom interactions. In this representation, Eq. (A2) becomes

$$\dot{\tilde{\sigma}}_{ge}^{\xi} + (\Gamma'/2 + i\lambda_\xi - i\Delta)\tilde{\sigma}_{ge}^{\xi} = i\tilde{\Omega}^{\xi}, \tag{A4}$$

where $\{\lambda_\xi\}$ are the eigenvalues of the Hamiltonian of Eq. (A1) in the single-excitation sector. The real $[J_\xi = \text{Re}(\lambda_\xi)]$ and imaginary $[\Gamma_\xi = -2\text{Im}(\lambda_\xi)]$ parts of these eigenvalues encode the frequency shift and collective decay rate of each of the modes. In the above equation, $\tilde{\sigma}_{ge}^{\xi} = \sum_{i=1}^{N} v_\xi^i \sigma_{ge}^{i}$, and $\tilde{\Omega}^{\xi} = \sum_{i=1}^{N} v_\xi^i \Omega_{ge}^{i}$ are linear combinations of the coherences and the field at the atomic positions, projected onto the eigenvectors $\mathbf{v}_\xi$. The dynamics is thus that of N independent dipoles.

If atoms are in the mirror configuration, there is a single bright mode with eigenvalue $\lambda_{\text{bright}} = -iN\Gamma_{1D}/2$. The above equation becomes

$$\dot{p} + (\Gamma'/2 + \text{OD}\Gamma'/4 - i\Delta)p = i\Omega_{\text{bright}}, \tag{A5}$$

where we have defined $p \equiv \tilde{\sigma}_{eg}^{\text{bright}}$. On resonance (with $\Delta = 0$), this equation is equivalent to the low-intensity and bad-cavity limits in the cavity QED work of Carmichael *et al.* [42].

All collective modes contribute to the output field if atoms are not in the mirror configuration. To calculate the output field, we use the transmission coefficient [40]

$$T(\omega) = 1 - \frac{i\Gamma_{1D}}{2}\sum_{\xi=1}^{N}\frac{\eta_\xi}{\omega - \omega_0 + i\Gamma'/2 - \lambda_\xi}, \tag{A6}$$

which is obtained by solving Eq. (A2) in the steady state and plugging the solution for the coherences in Eq. (A3). Here, $\{\eta_\xi\}$ are coefficients given in terms of the eigenvectors $\{\mathbf{v}_\xi\}$ as

$$\eta_\xi = \sum_{n=1}^{N}\sum_{m=1}^{N} v_{\xi,n}v_{\xi,m}e^{-ikd(n-m)}. \tag{A7}$$

We model the input pulse as a Gaussian with central frequency ω_p and standard deviation $\sigma = \text{FWHM}/2\sqrt{2\ln 2}$. Plugging Eq. (A6) into Eq. (1) yields

$$\begin{aligned}\frac{I_d(t)}{I_0} = \Bigg| & E_0(t)e^{-i\Delta t} - \frac{\Gamma_{1D}}{4} \\ & \times \sum_{\xi=1}^{N}\eta_\xi e^{-(\Gamma'+\Gamma_\xi)t/2}e^{-iJ_\xi t}e^{-\frac{1}{2}(\Delta+i\Gamma'/2-\lambda_\xi)^2\sigma^2} \\ & \times \text{erfc}\left(\frac{-i(\Delta + i\Gamma'/2 - \lambda_\xi)\sigma^2 - t}{\sqrt{2}\sigma}\right)\Bigg|^2,\end{aligned} \tag{A8}$$

where $\Delta \equiv \omega_p - \omega_0$. The coefficients a_ξ and b_ξ of Eq. (4) thus read

$$a_\xi = \eta_\xi e^{-\frac{1}{2}(\Delta+i\Gamma'/2-\lambda_\xi)^2\sigma^2}, \tag{A9a}$$

$$b_\xi = -i(\Delta + i\Gamma'/2 - \lambda_\xi)\sigma^2. \tag{A9b}$$

The coefficients η_ξ weight the contributions of different modes. The most superradiant modes have a larger coefficient and contribute more to the final signal.

For late times, we can approximate $\text{erfc}(\cdot) \sim 2$ for all the terms. Furthermore, we neglect the input field to determine the slope of the second peak and approximate the scattered field by the term corresponding to the first few most superradiant modes,

$$\frac{I_d(t)}{I_0} \propto \left|\sum_{\xi=1}^{\xi_{\text{cut}}}\tilde{\eta}_\xi e^{-(\Gamma'+\Gamma_\xi)t/2}e^{-iJ_\xi t}\right|^2. \tag{A10}$$

In the above equation, $\xi_{\rm cut} \in \mathbb{N}$ is a mode cutoff, and $\tilde{\eta}_\xi$ is a prefactor absorbing all the constants. The first few superradiant modes have a scaling $\Gamma_\xi \sim N\Gamma_{\rm 1D}$. We approximate $\Gamma_\xi \sim N\Gamma_{\rm 1D}$ and write

$$\frac{I_d(t)}{I_0} \propto e^{-(\Gamma'+N\Gamma_{\rm 1D})t}\left|\sum_{\xi=1}^{\xi_{\rm cut}} \tilde{\eta}_\xi e^{-\Delta_\xi t/2} e^{-iJ_\xi t}\right|^2. \tag{A11}$$

Here, Δ_ξ is a correction that arises from the approximation of Γ_ξ as $N\Gamma_{\rm 1D}$. Overall, $I_d(t) \propto I_0 e^{-(\Gamma'+N\Gamma_{\rm 1D})t}F(t)$, with $F(t)$ a function whose evolution timescale is much larger than $(\Gamma'+N\Gamma_{\rm 1D})^{-1}$. The effective decay rate at the second maximum is then approximately $\Gamma'+N\Gamma_{\rm 1D} = \Gamma'(1+\frac{\rm OD}{2})$. Note that this approximation becomes exact only for atoms in the mirror configuration.

3. Transmitted intensity in the continuous limit

Here we provide the derivation of Eq. (6) in the main text. Since $N \gg 1$, $\mathcal{T}_N(\omega)$ is well approximated by Eq. (5) of the main text [30]. Defining $z \equiv \omega - \omega_p$, we can write the output intensity from Eq. (1) as

$$\frac{I_d(t)}{I_0} = \left|\frac{1}{2\pi}\int_{-\infty}^{\infty} \exp\left(\frac{-iN\Gamma_{\rm 1D}}{2}\frac{1}{z+\Delta+i\Gamma'/2}\right)\exp\left(-\frac{1}{2}\sigma^2 z^2\right)\exp(-izt)dz\right|^2. \tag{A12}$$

Via the Bessel generating function,

$$\exp\left(\frac{-iN\Gamma_{\rm 1D}}{2}\frac{1}{z+\Delta+i\Gamma'/2} - izt\right) = e^{\left(i\Delta-\frac{\Gamma'}{2}\right)t}\sum_{m=-\infty}^{\infty}\left[-i\left(z+\Delta+i\frac{\Gamma'}{2}\right)\sqrt{\frac{2t}{N\Gamma_{\rm 1D}}}\right]^m \times J_m(\sqrt{2N\Gamma_{\rm 1D}t}), \tag{A13}$$

the output intensity can be expressed as the expansion given in Eq. (6). The expansion coefficients take the form

$$A_m = \frac{(-2i)^m}{2\pi}\int_{-\infty}^{\infty} dz\left(z+\Delta+i\frac{\Gamma'}{2}\right)^m e^{-\frac{1}{2}\sigma^2 z^2}. \tag{A14}$$

For $m > 0$, A_m can be written in terms of a confluent hypergeometric function of the second kind,

$$A_m = \frac{(2)^{m-1}}{\sqrt{\pi}}\left(\frac{2}{\sigma^2}\right)^{\frac{m+1}{2}} U\left(-\frac{1}{2}m;\frac{1}{2};-\frac{\sigma^2\left(\Delta+i\frac{\Gamma'}{2}\right)^2}{2}\right). \tag{A15}$$

For $m < 0$,

$$A_m = \frac{(-2i)^m}{2\pi}\frac{(-1)^{|m|-1}}{(|m|-1)!}\partial_\alpha^{|m|-1}F(\alpha,\sigma)\big|_{\alpha=\Delta+i\frac{\Gamma'}{2}}, \tag{A16}$$

with

$$F(\alpha,\sigma) = -i\pi e^{-\frac{1}{2}\sigma^2\alpha^2}\left[\mathrm{erf}\left(i\frac{\alpha\sigma}{\sqrt{2}}\right)+1\right]. \tag{A17}$$

APPENDIX B: ABSORPTION SPECTRUM

The optical dipole trap produces position-dependent light shifts. The wavelengths are near almost magic, but the slight difference from the magic condition produces a small residual effect. Our knowledge of the polarization *in situ* is not perfect; we do expect some residual longitudinal circular polarization, which creates an artificial magnetic field causing shifts. We do not optically pump all the atoms into a single Zeeman sublevel to increase the control of this effect, and it is probably the cause of broadening. The nonharmonicity of the trap and the fact that the atoms are not at the trap ground state also contribute to the asymmetry. The transmission coefficient, given by the Beer-Lambert law, of the actual atomic sample departs from the exponential of a Lorentzian distribution, as in Eq. (3) of the main text. As a result, the absorption spectrum (i.e., the transmittance) can often look broadened and even asymmetric.

The details of the position distribution of the atoms and position-dependent light shifts are not directly measurable and difficult to estimate. We have the measured transmittance of the intensity, but we need that of the field with its real and imaginary components. We use a phenomenological approach to describe the absorption coefficient of the total atomic sample, $\mathcal{T}(\omega)$, by considering it as an ensemble of smaller samples with optical density OD_i that is frequency shifted by ω_i with transmission coefficient $\mathcal{T}_i(\omega,\omega_i,\mathrm{OD}_i)$. This is $\mathcal{T}(\omega) = \prod_i \mathcal{T}_i(\omega,\omega_i,\mathrm{OD}_i)$. All the shifts are randomly distributed, as we assume that the position distribution is random within the traps but bounded to a maximum shift on one side of the spectrum, a process characterized by log-normal distributions.

Figure 4 presents an example of a few light-shifted transmission spectra sampled over a log-normal distribution that produce an asymmetrically broadened transmission spectrum

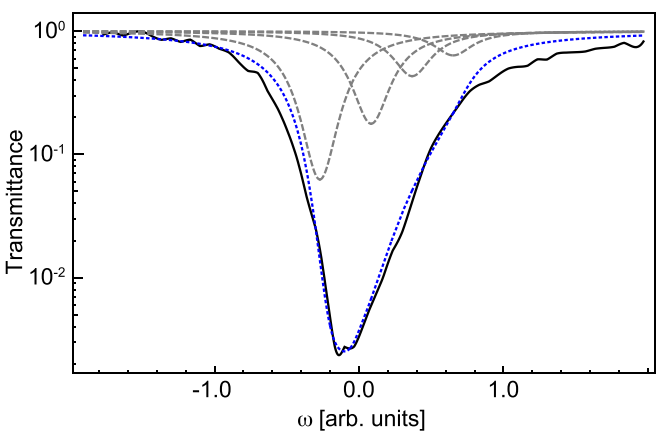

FIG. 4. Comparison of the measured transmittance (solid black in logarithmic scale) with the modeled one (dotted blue). The model consists of a sum of frequency-shifted Lorentzian spectra (dashed gray) log-normally distributed.

close to the measured one. In this case, the modeled transmission spectrum was adjusted to overlap with the measured spectrum, while in the main text, it was adjusted to better predict the transmitted pulse. A different number of subsamples, shifts, and shapes of the log-normal distribution produces similar pulse intensity outputs as long as the transmittance roughly overlaps with the measured one. These results suggest that an approximate model is enough to reproduce the transmitted pulse shape, even when the actual absorption coefficient is unknown.

APPENDIX C: DATA PROCESSING

The pulse transmission raw data obtained by photon counting on the SPCM has a background with no atoms of 1.5×10^{-3} of the peak height. The equivalent background with atoms is closer to 0.5×10^{-3}. We have adjusted the background (adding an average of 10 counts to every bin with its appropriate noise) in Fig. 3 to make the traces converge to the same long-term average value. The theoretical predictions have also had the background adjusted. The results of Fig. 3 are independent of this correction.

[1] H. Pichler, S. Choi, P. Zoller, and M. D. Lukin, Universal photonic quantum computation via time-delayed feedback, Proc. Natl. Acad. Sci. USA **114**, 11362 (2017).

[2] H. Zheng, D. J. Gauthier, and H. U. Baranger, Waveguide-QED-based photonic quantum computation, Phys. Rev. Lett. **111**, 090502 (2013).

[3] F. Ciccarello, D. E. Browne, L. C. Kwek, H. Schomerus, M. Zarcone, and S. Bose, Quasideterministic realization of a universal quantum gate in a single scattering process, Phys. Rev. A **85**, 050305(R) (2012).

[4] Y. Zhan and S. Sun, Deterministic generation of loss-tolerant photonic cluster states with a single quantum emitter, Phys. Rev. Lett. **125**, 223601 (2020).

[5] A. Sommerfeld, On the propagation of light in dispersing media, Ann. Phys. **349**, 177 (1914).

[6] L. Brillouin, On the propagation of light in dispersing media, Ann. Phys. **349**, 203 (1914).

[7] L. Brillouin, *Wave Propagation and Group Velocity* (Academic, San Diego, 1960).

[8] K. E. Oughstun and G. C. Sherman, *Electromagnetic Pulse Propagation in Causal Dielectrics* (Springer, Verlag, 1994).

[9] B. Macke and B. Ségard, Optical precursors in transparent media, Phys. Rev. A **80**, 011803(R) (2009).

[10] B. Macke and B. Ségard, Simple asymptotic forms for Sommerfeld and Brillouin precursors, Phys. Rev. A **86**, 013837 (2012).

[11] B. Macke and B. Ségard, From Sommerfeld and Brillouin forerunners to optical precursors, Phys. Rev. A **87**, 043830 (2013).

[12] K. Toyoda, Y. Takahashi, K. Ishikawa, and T. Yabuzaki, Optical free-induction decay of laser-cooled ^{85}Rb, Phys. Rev. A **56**, 1564 (1997).

[13] H. Jeong, A. M. C. Dawes, and D. J. Gauthier, Direct observation of optical precursors in a region of anomalous dispersion, Phys. Rev. Lett. **96**, 143901 (2006).

[14] S. Jennewein, M. Besbes, N. J. Schilder, S. D. Jenkins, C. Sauvan, J. Ruostekoski, J.-J. Greffet, Y. R. P. Sortais, and A. Browaeys, Coherent scattering of near-resonant light by a dense microscopic cold atomic cloud, Phys. Rev. Lett. **116**, 233601 (2016).

[15] S. Jennewein, L. Brossard, Y. R. P. Sortais, A. Browaeys, P. Cheinet, J. Robert, and P. Pillet, Coherent scattering of near-resonant light by a dense, microscopic cloud of cold two-level atoms: Experiment versus theory, Phys. Rev. A **97**, 053816 (2018).

[16] C. Möhl, N. L. R. Spong, Y. Jiao, C. So, T. Ilieva, M. Weidemüller, and C. S. Adams, Photon correlation transients in a weakly blockaded Rydberg ensemble, J. Phys. B: At., Mol. Opt. Phys. **53**, 084005 (2020).

[17] A. Padrón-Brito, R. Tricarico, P. Farrera, E. Distante, K. Theophilo, D. Chang, and H. de Riedmatten, Transient dynamics of the quantum light retrieved from Rydberg polaritons, New J. Phys. **23**, 063009 (2021).

[18] F. J. Lynch, R. E. Holland, and M. Hamermesh, Time dependence of resonantly filtered gamma rays from Fe^{57}, Phys. Rev. **120**, 513 (1960).

[19] S. M. Harris, Quantum mechanical calculation of Mössbauer transmission, Phys. Rev. **124**, 1178 (1961).

[20] U. van Bürck, Coherent pulse propagation through resonant media, Hyperfine Interact. **123/124**, 483 (1999).

[21] J. B. Hastings, D. P. Siddons, U. van Bürck, R. Hollatz, and U. Bergmann, Mössbauer spectroscopy using synchrotron radiation, Phys. Rev. Lett. **66**, 770 (1991).

[22] M. D. Crisp, Propagation of small-area pulses of coherent light through a resonant medium, Phys. Rev. A **1**, 1604 (1970).

[23] M. D. Crisp, Propagation of small-area pulses of coherent light through a resonant medium, Phys. Rev. A **2**, 2172 (1970).

[24] C. G. B. Garrett and D. E. McCumber, Propagation of a Gaussian light pulse through an anomalous dispersion medium, Phys. Rev. A **1**, 305 (1970).

[25] B. W. Adams, Nuclear γ-ray superradiance, J. Mod. Opt. **56**, 1974 (2009).

[26] A. A. Svidzinsky and M. O. Scully, Evolution of collective N atom states in single photon superradiance: Effect of virtual Lamb shift processes, Opt. Commun. **282**, 2894 (2009).

[27] Ralf Röhlsberger, Kai Schlage, Balaram Sahoo, Sebastien Couet, and Rudolf Rüffer, Collective Lamb shift in single-photon superradiance, Science **328**, 1248 (2010).

[28] S. Okaba, D. Yu, L. Vincetti, F. Benabid, and H. Katori, Superradiance from lattice-confined atoms inside hollow core fibre, Commun. Phys. **2**, 136 (2019).

[29] A. S. Sheremet, M. I. Petrov, I. V. Iorsh, A. V. Poshakinskiy, and A. N. Poddubny, Waveguide quantum electrodynamics: Collective radiance and photon-photon correlations, Rev. Mod. Phys. **95**, 015002 (2023).

[30] S. Cardenas-Lopez, P. Solano, L. A. Orozco, and A. Asenjo-Garcia, Optical precursors in waveguide quantum electrodynamics, Phys. Rev. Res. **5**, 013133 (2023).

[31] R. Pennetta, M. Blaha, A. Johnson, D. Lechner, P. Schneeweiss, J. Volz, and A. Rauschenbeutel, Collective radiative dynamics of an ensemble of cold atoms coupled to an optical waveguide, Phys. Rev. Lett. **128**, 073601 (2022).

[32] R. Pennetta, D. Lechner, M. Blaha, A. Rauschenbeutel, P. Schneeweiss, and J. Volz, Observation of coherent coupling between super- and subradiant states of an ensemble of cold atoms collectively coupled to a single propagating optical mode, Phys. Rev. Lett. **128**, 203601 (2022).

[33] J. Kumlin, K. Kleinbeck, N. Stiesdal, H. Busche, S. Hofferberth, and H. P. Büchler, Nonexponential decay of a collective excitation in an atomic ensemble coupled to a one-dimensional waveguide, Phys. Rev. A **102**, 063703 (2020).

[34] P. Solano, J. A. Grover, J. E. Hoffman, S. Ravets, F. K. Fatemi, L. A. Orozco, and S. L. Rolston, *Optical Nanofibers: A New Platform for Quantum Optics* (Academic Press, San Diego, 2017), Chap. 7, pp. 439–505.

[35] J. E. Hoffman, S. Ravets, J. A. Grover, P. Solano, P. R. Kordell, J. D. Wong-Campos, L. A. Orozco, and S. L. Rolston, Ultrahigh transmission optical nanofibers, AIP Adv. **4**, 067124 (2014).

[36] E. Vetsch, D. Reitz, G. Sagué, R. Schmidt, S. T. Dawkins, and A. Rauschenbeutel, Optical interface created by laser-cooled atoms trapped in the evanescent field surrounding an optical nanofiber, Phys. Rev. Lett. **104**, 203603 (2010).

[37] A. Goban, K. S. Choi, D. J. Alton, D. Ding, C. Lacroûte, M. Pototschnig, T. Thiele, N. P. Stern, and H. J. Kimble, Demonstration of a state-insensitive, compensated nanofiber trap, Phys. Rev. Lett. **109**, 033603 (2012).

[38] D. Ding, A. Goban, K. S. Choi, and H. J. Kimble, Corrections to our results for optical nanofiber traps in cesium, arXiv:1212.4941.

[39] F. Le Kien, P. Schneeweiss, and A. Rauschenbeutel, Dynamical polarizability of atoms in arbitrary light fields: General theory and application to cesium, Eur. Phys. J. D **67**, 92 (2013).

[40] A. Asenjo-Garcia, J. D. Hood, D. E. Chang, and H. J. Kimble, Atom-light interactions in quasi-one-dimensional nanostructures: A Green's-function perspective, Phys. Rev. A **95**, 033818 (2017).

[41] P. Solano, P. Barberis-Blostein, F. K. Fatemi, L. A. Orozco, and S. L. Rolston, Super-radiance reveals infinite-range dipole interactions through a nanofiber, Nat. Commun. **8**, 1857 (2017).

[42] H. J. Carmichael, R. J. Brecha, and P. R. Rice, Quantum interference and collapse of the wave function in cavity QED, Opt. Commun. **82**, 73 (1991).

[43] I. H. Deutsch, R. J. C. Spreeuw, S. L. Rolston, and W. D. Phillips, Photonic band gaps in optical lattices, Phys. Rev. A **52**, 1394 (1995).

[44] N. V. Corzo, B. Gouraud, A. Chandra, A. Goban, A. S. Sheremet, D. V. Kupriyanov, and J. Laurat, Large Bragg reflection from one-dimensional chains of trapped atoms near a nanoscale waveguide, Phys. Rev. Lett. **117**, 133603 (2016).

[45] H. L. Sørensen, J.-B. Béguin, K. W. Kluge, I. Iakoupov, A. S. Sørensen, J. H. Müller, E. S. Polzik, and J. Appel, Coherent backscattering of light off one-dimensional atomic strings, Phys. Rev. Lett. **117**, 133604 (2016).

[46] B. D. Patterson, P. Solano, P. S. Julienne, L. A. Orozco, and S. L. Rolston, Spectral asymmetry of atoms in the van der Waals potential of an optical nanofiber, Phys. Rev. A **97**, 032509 (2018).

[47] D. Su, P. Solano, J. D. Wack, L. A. Orozco, and Y. Zhao, Torsional optomechanical cooling of a nanofiber, Photon. Res. **10**, 601 (2022).